Stanford Exploration Project, Report 120, May 3, 2005, pages 333–347

A self-adaptive algorithm for choosing reference velocities in the presence of lateral velocity variations

Huazhong Wang and Guojian Shan[1]

ABSTRACT

Seismic wave propagation depicted with the perturbation theory has important and widespread uses in reflection seismology. As we know, in perturbation theory, wave propagation needs a reference velocity. The closer the reference velocity is to the true velocity, the more accurate the wave propagation is. However, it is not easy to choose reasonable reference velocities in the presence of severe lateral velocity variations. Assigning a reference velocity value at each spatial point is not computationally feasible, because there is a trade-off between the calculation cost and the number of reference velocities. We show that the accuracy of seismic wave propagation can be more easily improved by choosing a set of reasonable reference velocities rather than by optimizing a one-way wave propagator. Therefore, we introduce a self-adaptive approach to choose a set of reference velocities for an extrapolation layer, in the presence of lateral velocity variations. Through sorting the velocity data an array with increasing values, and by setting a threshold average-velocity ratio or velocity- variance ratio, we can choose a set of reasonable reference velocities for wavefield extrapolation. This method can also be used for image edge detecting. It is flexible and computationally cost-effective.

INTRODUCTION

Seismic migration is used to image recorded reflection and scatter events based on wave theoretical approaches, by de-propagating them to their true subsurface positions. Wave propagation and de-propagation is based on perturbation theory. Nowadays, prestack depth migration (**PSDM**) has become a most effective tool for imaging complex geological structures. Assuming the macro-velocity field is accurate enough, the migration operators or wave propagators should be competent for accurately expressing wave propagation in media with severe lateral velocity variations.

Stoffa et al. (1990) introduced a first-order split-step correction, which is accurate for flat reflectors. However, the accuracy of the migration operator for depicting wave propagation decreases as reflectors become steeper and the differences between the reference and migration velocities increase. Therefore, Ristow and Ruhl (1994) put forward the Fourier finite-difference (FFD) operator, and Huang et al. (1999) and Rousseau and de Hoop (2001) intro-

[1]**email:** wang@sep.stanford.edu, shan@sep.stanford.edu

duced the generalized-screen propagator GSP, to compensate for high-order terms neglected when imaging steeply dipping reflectors with the Split-Step Fourier SSF operator. The FFD operator deals with the high-order terms in the frequency-space domain; the GSP processes them in the frequency-wavenumber domain. The FFD operator requires that the reference velocity is lower than the minimum velocity in an extrapolation layer, because the sign of the coefficients in the finite-difference equation can not be changed at different lateral points in a depth layer. Otherwise, calculation instability will occur. Therefore, even if a set of suitable reference velocities is given, the FFD operator cannot give a very good image.

Biondi (2002) modified the general FFD operator by introducing the interpolation of two wavefields: the first wavefield is obtained by applying the FFD correction, starting from a reference velocity lower than the medium velocity; the second wavefield is obtained by applying the FFD correction starting from a reference velocity higher than the medium velocity.

In fact, the high-order terms in wave-propagation perturbation theory are generated by the velocity perturbation between the true velocity and the reference velocity. If the reference velocity is chosen as close as possible to the true velocity, the SSF, FFD and GSP operators can accurately characterize the wave propagation in media with severe lateral velocity variations. Futhermore, the imaging quality can be improved with such propagators.

Assuming that the macro-velocity model for imaging is accurate enough, the main reason for most imaging errors is that the *one-way wave equation can not accurately characterize the wave propagation in the case of severe lateral velocity variations*. In such cases, steeply dipping reflectors cannot be clearly imaged. We can decrease these errors either by using an optimized, but complex propagator, or by choosing a set of reasonable reference velocities and using a simple propagator. We think that the latter is much more flexible and cost-effective. Of course, both approaches can be combined together.

Clapp (2004) proposed that the reference velocity can be selected by a generalized Lioyd method. The basic idea behind Lioyd's method is to iteratively improve the quantization of a function by looking at the velocity statistics of each region (such as mean, median, and variance), and then changing the boundaries of the regions at each iteration to find the solution which is optimal based on some criterion.

Now, we introduce a self-adaptive strategy for selecting a reasonable reference velocity in the presence of lateral velocity variations. The main steps include setting a threshold for the ratio between two adjoining reference velocities, sorting the velocity slice into an array, and detecting the edges of velocity regions using velocity averages and variances in the different regions. The resulting reference velocity field and the imaging results produced with it indicate that our approach is correct and effective. Meanwhile, the method is flexible in use, computationally efficient, and easy to program in either 2D or 3D. The approach can also be used for 2D or 3D image edge detecting. Numerical tests demenstrate that the method is effective.

WAVE PROPAGATOR CHARACTERIZED BY PERTURBATION THEORY

The Single-Square-Root (**SSR**) wavefield-extrapolation equation in the case of lateral velocity variation is of the following form (Claerbout, 1985):

$$\frac{\partial P(t,x,y,z)}{\partial z} = \pm \left[\frac{1}{v^2(x,y,z)} - \left(\frac{\partial t}{\partial x}\right)^2 - \left(\frac{\partial t}{\partial y}\right)^2 \right]^{\frac{1}{2}} \frac{\partial P(t,x,y,z)}{\partial t}. \tag{1}$$

The sign convention for the square root is negative for upcoming wavefield and positive for downgoing wavefield. We decompose the velocity field into two parts: the background velocity field and the velocity perturbation. In fact, we process the slowness field because the decomposition of the slowness is linear. The slowness field decomposition is defined as follows:

$$S(x,y,z) = \frac{1}{v(x,y,z)} = \frac{1}{v(z)} + \triangle S(x,y,z) = S_0(z) + \triangle S(x,y,z), \tag{2}$$

where$S_0(z)$ is the background slowness, $v(z)$ the background velocity and $\triangle S(x,y,z)$ is the slowness perturbation. We hope that the velocity perturbation $\triangle S(x,y,z)$ is as small as possible. Substituting the slowness-field-decomposition equation (2) into the wavefield-depth-extrapolation equation (1) and discarding the second-order terms of the slowness perturbation yields the following formula:

$$\frac{\partial P(t,x,y,z)}{\partial z} = \pm \left[\frac{1}{v^2(z)} + 2S_0(z)\triangle S(x,y,z) - \left(\frac{\partial t}{\partial x}\right)^2 - \left(\frac{\partial t}{\partial y}\right)^2 \right]^{\frac{1}{2}} \frac{\partial P(t,x,y,z)}{\partial t}. \tag{3}$$

Equation (3) can be rewritten as follows:

$$\frac{\partial P(t,x,y,z)}{\partial z} = \pm \left\{ \sqrt{\frac{1}{v^2(z)} - \left(\frac{\partial t}{\partial x}\right)^2 - \left(\frac{\partial t}{\partial y}\right)^2} \sqrt{1 + \frac{2S_0(z)(z)\triangle S(x,y,z)}{\frac{1}{v^2(z)} - \left(\frac{\partial t}{\partial x}\right)^2 - \left(\frac{\partial t}{\partial y}\right)^2}} \right\} \frac{\partial P(t,x,y,z)}{\partial t}. \tag{4}$$

In simplicity, we define $A = \sqrt{\frac{1}{v^2(z)} - \left(\frac{\partial t}{\partial x}\right)^2 - \left(\frac{\partial t}{\partial y}\right)^2}$. Taylor-series expansion of the second square-root term in equation (4), neglecting second- and higher-order terms, yields

$$\frac{\partial P(t,x,y,z)}{\partial z} \approx \pm \left\{ A + \frac{S_0(z)\triangle S(x,y,z)}{A} \right\} \frac{\partial P(t,x,y,z)}{\partial t}. \tag{5}$$

Meanwhile, equation (5) can be rearranged as follows:

$$\begin{aligned} \frac{\partial P(t,x,y,z)}{\partial z} = & \pm [A] \frac{\partial P(t,x,y,z)}{\partial t} \\ & \pm \frac{S_0(z)}{A} \frac{\partial \left[\triangle S(x,y,z) P(t,x,y,z)\right]}{\partial t}. \end{aligned} \tag{6}$$

Transforming equation (6) into frequency-wavenumber domain gives

$$\frac{\partial P\left(\omega,k_x,k_y;z\right)}{\partial z}=\mp ik_0k_zP\left(\omega,k_x,k_y;z\right)\mp\frac{i}{k_z}FT_{x,y}\left[\omega\triangle S(x,y,z)\,P\left(\omega,x,y;z\right)\right], \quad (7)$$

where $k_0=\frac{\omega}{v(z)}$, $k_z=\sqrt{1-\left(\frac{k_T}{k_0}\right)^2}$, $k_T=\sqrt{k_x^2+k_y^2}$. Equation (7) can be split into two equations:

$$\frac{\partial P\left(\omega,k_x,k_y;z\right)}{\partial z}=\mp ik_0k_zP\left(\omega,k_x,k_y;z\right) \quad (8)$$

and

$$\frac{\partial P\left(\omega,k_x,k_y;z\right)}{\partial z}=\mp\frac{i}{k_z}FT_{x,y}\left[\omega\triangle S(x,y,z)\,P\left(\omega,x,y;z\right)\right]. \quad (9)$$

Equation (8) downward extrapolates the wave field in the background velocity. Equation (9) describes the scattering wave propagation, which is caused by the slowness perturbation. The total wavefield is the summation of the background and scattering wavefields. When the vertical wavenumber k_z approaches zero, equation (9) has a singular point. To circumvent the problem, $\frac{1}{k_z}$ is expanded into a Taylor series:

$$\begin{aligned}\frac{1}{k_z} &= \frac{1}{\sqrt{1-\left(\frac{k_T}{k_0}\right)^2}}=1+\frac{1}{2}\left(\frac{k_T}{k_0}\right)^2+\frac{1\cdot3}{2\cdot4}\left(\frac{k_T}{k_0}\right)^4+\cdots+\frac{(2n-1)!!}{2^n\,(n)!!}\left(\frac{k_T}{k_0}\right)^{2n}+\cdots\\ &= 1+\sum_{n=1}^{\infty}\frac{(2n-1)!!}{2^n}\left(\frac{k_T}{k_0}\right)^{2n}. \quad (10)\end{aligned}$$

Substituting formula (10) into equation (9) gives,

$$\begin{aligned}\frac{\partial P\left(\omega,k_x,k_y,z\right)}{\partial z} &= \mp i\left\{1+\sum_{n=1}^{\infty}\frac{(2n-1)!!}{2^n}\left(\frac{k_T}{k_0}\right)^{2n}\right\}FT_{x,y}\left[\omega\triangle S(x,y,z)\,P\left(\omega,x,y;z\right)\right]\\ &= \mp iFT_{x,y}\left[\omega\triangle S(x,y,z)\,P\left(\omega,x,y;z\right)\right]\\ &\mp i\sum_{n=1}^{\infty}\frac{(2n-1)!!}{2^n}\left(\frac{k_T}{k_0}\right)^{2n}FT_{x,y}\left[\omega\triangle S(x,y,z)\,P\left(\omega,x,y;z\right)\right]. \quad (11)\end{aligned}$$

Equation (11) is also split into two equations:

$$\frac{\partial P\left(\omega,x,y,z\right)}{\partial z}=\mp i\omega\triangle S(x,y,z)\,P\left(\omega,x,y;z\right) \quad (12)$$

and

$$\frac{\partial P\left(\omega,k_x,k_y,z\right)}{\partial z}=\mp i\sum_{n=1}^{\infty}\frac{(2n-1)!!}{2^n}\left(\frac{k_T}{k_0}\right)^{2n}FT_{x,y}\left[\omega\triangle S(x,y,z)\,P\left(\omega,x,y;z\right)\right]. \quad (13)$$

In the case of narrow propagation angles (near zero degree), $\frac{1}{k_z} \approx 1$ is satisfied, and equations (8) and (9) degrade to the split-step Fourier propagator (Stoffa, 1990):

$$\frac{\partial P\left(\omega, k_x, k_y; z\right)}{\partial z} = \mp i k_0 k_z P\left(\omega, k_x, k_y; z\right), \tag{14}$$

$$\frac{\partial P\left(\omega, x, y; z\right)}{\partial z} = \mp i \omega \triangle S(x, y, z) P\left(\omega, x, y; z\right). \tag{15}$$

Equations (8), (12) and (13) are combined to form the GSP (Huang et al, 1999). We can see that equation (13) deals with the wave propagation at high angles, which can be processed in either the frequency wavenumber domain (with the GSP operator) or frequency space domain (with the FFD operator). From the above derivation, we can see that the high-order terms of the slowness perturbation have been discarded twice, which works only under the condition of small slowness perturbation. Therefore, the slowness perturbation $\triangle S(x, y, z)$ should be as small as possible. However, using the velocity value at each spatial point as a reference velocity is impractical in calculation. Generally, the slowness perturbation is defined as

$$\triangle S\left(x_i, y_j, z\right) = S\left(x_i, y_j, z\right) - S_0(z) \tag{16}$$

We need to choose a set of reference velocities in an extrapolation step to maximize the accuracy of wave propagation.

SELF-ADAPTIVE REFERENCE VELOCITY CHOICE WITH LATERAL VELOCITY VARIATIONS

The background velocity or reference velocity should be chosen to match the true velocity distribution as closely as possible. The more closely the reference velocity field mimics the true velocity, the more accurately the wave-field propagation can be calculated and the higher the modeling and imaging quality will be. We redefine the velocity perturbation as

$$\triangle S\left(x_i, y_j, z\right) = S\left(x_i, y_j, z\right) - S_0^l\left(x_i, y_j, z\right), \tag{17}$$

where l is the index of the selected reference velocity. $S_0^l\left(x_i, y_j, z\right)$ means that there is a reference velocity with the index l at a spatial point $\left(x_i, y_j\right)$. In the extreme case, the maximum number of the reference velocities equals to the number of discrete spatial points in the extrapolation layer. Theoretically, every spatial point could be assigned a reference velocity, but that would entail a huge calculation cost. Generally, a set of reference velocities is chosen, with which the wavefield extrapolations are carried out. Then the extrapolated wavefields are merged together with some chosen methods (Gazdag and Sguazzero, 1984; Kessinger, 1992). However, it is difficult to choose a set of reasonable reference velocities for modeling and imaging, if the velocity laterally varies severely and irregularly. Therefore, we propose the following self-adaptive strategy for medium with lateral velocity variations. The procedure is as follows:

(1) Assign a threshold value of the ratio of two adjoining reference velocities, according to numerical experiments and experience. The threshold reflects how severe the lateral velocity variation is. Generally, we define the ratio to be greater than 1.0. Of course the threshold could be less than 1.0, but this would require sorting the discrete velocity values in decreasing order in the third step.

(2) Filter the 2D or 3D velocity slice of the depth layer with a median filter to eliminate possible wild velocity values.

(3) Sort the discrete velocity values into an array in increasing order.

(4) Set the summation value equal to zero, then sum the sorted discrete velocity values from left to right and point-by-point, calculating a cumulative velocity average, if a velocity value is added, with the formula $v^l_{avg} = \frac{\sum_{k=1}^{K^l} v_k^{\tilde{m}}(x_i, y_j)}{K^l}$. Here, $\tilde{m} = 1, ..., NX$ in the 2D case and $\tilde{m} = 1, ..., NX \times NY$ in the 3D case, where $\tilde{m}$ are the sequence numbers of the discrete velocity points that were disordered by sorting. K^l is the number of discrete velocity points in the l^{th} region, which is known after a dividing point is determined; l is the number of the reference velocity. If the ratio between the velocity value at the next point and the velocity average at the current point is greater than the preset threshold, we can judge that there exists a velocity boundary at the current point. This point is a dividing point between two velocity regions.

(5) Starting from the dividing point, repeat Step 4 to finding each successive dividing point until the end of the sorted velocity array is reached.

(6) Repeat Step 4 and Step 5. This time, the ratio between the cumulative velocity average at the current point and the velocity average at the adjacent and next point (which is calculated in the last iteration) is used, and if it is greater than the preset threshold value, the dividing point between two velocity regions is determined.

(7) If the velocity dividing points are not changed and the velocity averages are not changed, stop the iterative procedure. Otherwise, repeat Step 6.

We can see that the number of velocity regions is the number of chosen reference velocities. The velocity average in a velocity region is a reference velocity value. With the set of reference velocities, wavefield extrapolation is carried out with SSF, FFD, or GSP operators. For computational efficiency, the number of reference velocities should be kept small, usually less than 5 or 6. It should be mentioned that Step 6 and 7 are optional.

In order to merge extrapolated wavefield, the corresponding sequence number between the input discrete velocity slice and the sorted discrete velocity value should be recorded. This is important for the approach.

The approach can be used in 2D or 3D, poststack or prestack, and time or depth migration or modeling, as long as the seismic-wave propagation is characterized with perturbation theory. This method can be used for the image edge detecting as well.

If necessary, the velocity variances may be used as the criterion for dividing the velocity regions. Usualy, it is sufficient to choose a set of reference velocities with velocity averages

for migration.

WAVEFIELD RECONSTRUCTION

Gazdag and Sguazzero (1984) use the following method for merging the extrapolated wavefield. Assume that the two extrapolated wavefields with the different reference velocities v^1_{ref} and v^2_{ref} are as follows:

$$P_1\left(x_i, y_j, z+\triangle z; \omega\right) = A_1 e^{i\theta_1}, \tag{18}$$

$$P_2\left(x_i, y_j, z+\triangle z; \omega\right) = A_2 e^{i\theta_2}, \tag{19}$$

where A_1 and A_2, and θ_1 and θ_2 represent amplitude and phase, respectively. The merged wavefield at a spatial point is

$$P\left(x_i, y_j, z+\triangle z; \omega\right) = A e^{i\theta}. \tag{20}$$

The amplitude and phase of the merged wavefield is cauculated with

$$A = \frac{A_1\left(v^2_{ref} - v\left(x_i, y_j, z+\triangle z\right)\right) + A_2\left(v\left(x_i, y_j, z+\triangle z\right) - v^1_{ref}\right)}{v^2_{ref} - v^1_{ref}}, \tag{21}$$

and

$$\theta = \frac{\theta_1\left(v^2_{ref} - v\left(x_i, y_j, z+\triangle z\right)\right) + \theta_2\left(v\left(x_i, y_j, z+\triangle z\right) - v^1_{ref}\right)}{v^2_{ref} - v^1_{ref}}. \tag{22}$$

where $v\left(x_i, y_j, z+\triangle z\right)$ is the velocity at the spatial point $\left(x_i, y_j, z+\triangle z\right)$. Kessinger (1992) shows that the wavefield at a spatial point can be directly replaced by the extrapolated wavefield with the reference velocity corresponding to the spatial point. The following formula is used for merging the extrapolated wavefields with SSF operator

$$\begin{aligned} P\left(x_i, y_j, z+\triangle z; \omega\right) &= \delta\left(v_{ref}\left(x_i, y_j, z+\triangle z\right) - v^l_{ref}\right) e^{i\triangle s\left(x_i, y_j, z+\triangle z\right)\triangle z} \\ &\quad FFT^{-1}\left[e^{ik_z\triangle z} P\left(x_i, y_j, z+\triangle z; \omega\right)\right], \end{aligned} \tag{23}$$

where $v_{ref}\left(x_i, y_j, z+\triangle z\right)$ stands for the reference velocity at a spatial point $\left(x_i, y_j\right)$, v^l_{ref} is the member of the set of chosen reference velocities with the index l. The delta function $\delta(\bullet) = 1$ if $v_{ref}\left(x_i, y_j, z+\triangle z\right) = v^l_{ref}$; otherwise, $\delta(\bullet) = 0$. With this method, the extrapolated wavefield can be directly inserted into the relevant position without storing it. However, the amplitude and phase of the merged wavefield is not so accurate in the case of severe lateral velocity variations. We use quadratic interpolation to reconstruct the extrapolated wavefield with the

following equation:

$$P\left(x_i,y_j,z+\triangle z;\omega\right)= \tag{24}$$
$$\delta\left(v_{ref}\left(x_i,y_j,z+\triangle z\right)-v_{ref}^{l}\right)\left\{\begin{array}{l}\frac{\left(v(x_i,y_j)-v_{ref}^{l}\right)\left(v(x_i,y_j)-v_{ref}^{l+1}\right)}{\left(v_{ref}^{l-1}-v_{ref}^{l}\right)\left(v_{ref}^{l-1}-v_{ref}^{l+1}\right)}P^{l-1}\left(x_i,y_j,z+\triangle z;\omega\right)\\ +\frac{\left(v(x_i,y_j)-v_{ref}^{l-1}\right)\left(v(x_i,y_j)-v_{ref}^{l+1}\right)}{\left(v_{ref}^{l}-v_{ref}^{l-1}\right)\left(v_{ref}^{l}-v_{ref}^{l+1}\right)}P^{l}\left(x_i,y_j,z+\triangle z;\omega\right)\\ +\frac{\left(v(x_i,y_j)-v_{ref}^{l-1}\right)\left(v(x_i,y_j)-v_{ref}^{l}\right)}{\left(v_{ref}^{l+1}-v_{ref}^{l-1}\right)\left(v_{ref}^{l+1}-v_{ref}^{l}\right)}P^{l+1}\left(x_i,y_j,z+\triangle z;\omega\right)\end{array}\right\},$$

where $P^{l-1}\left(x_i,y_j,z+\triangle z;\omega\right)$, $P^{l}\left(x_i,y_j,z+\triangle z;\omega\right)$ and $P^{l+1}\left(x_i,y_j,z+\triangle z;\omega\right)$ are the extrapolated wavefield at point $\left(x_i,y_j\right)$ with the three adjacent reference velocities v_{ref}^{l-1}, v_{ref}^{l} and v_{ref}^{l+1}, respectively.

NUMERICAL TEST EXAMPLES

Now, we show some numerical examples of poststack depth migration results with the SSF operator, in which the reference velocity is chosen with the approach discussed above. Figure 1 is the 2D SEG/EAGE salt-dome model. Figure 2 shows the imaging result generated with the (**SSF**) operator with one reference velocity during one extrapolation step. The image is very noisy, especially in the inner part of the salt dome, and the small faults are vague and difficult to identify. In Figure 4, the reference velocity is chosen with the approach presented above, and the threshold of the ratio between two adjacent velocity steps is set to 1.3. We can see that the imaging noise is greatly attenuated, and the faults and the boundary are quite clear. Figure 3 and Figure 5 are similar to Figure 4, but with a threshold of 1.5 and 1.1. In Figure 5, the imaging quality is improved further, but the improvement is not sufficient to justify the increased number of reference velocities. In Figure 3, the imaging quality is not decreased obviously, which means that it is not necessary for the number of reference velocities to be too much. The reason why the noise appears on the right part of these images does not figure out. It remains a problem. The chosen reference velocity field, with the threshold set to 1.5, 1.3 and 1.1, is shown in Figure 6, 7, and 8, respectively. This choice satisfactorily characterizes the background variation of the true 2D SEG/EAGE salt-dome velocity model.

CONCLUSION AND DISCUSSION

We introduce the self-adaptive approach for choosing a set of reference velocities. The approach is quite flexible and of little calculation cost. It can be used for general image edge-detecting also. Numerical tests demenstrate that the method is effective. During the wavefield extrapolation, the wavefield merging remains a problem in the case of severe lateral velocity variation. Furthermore, by considering the velocity variance in a region, a better reference velocity choice can be reached.

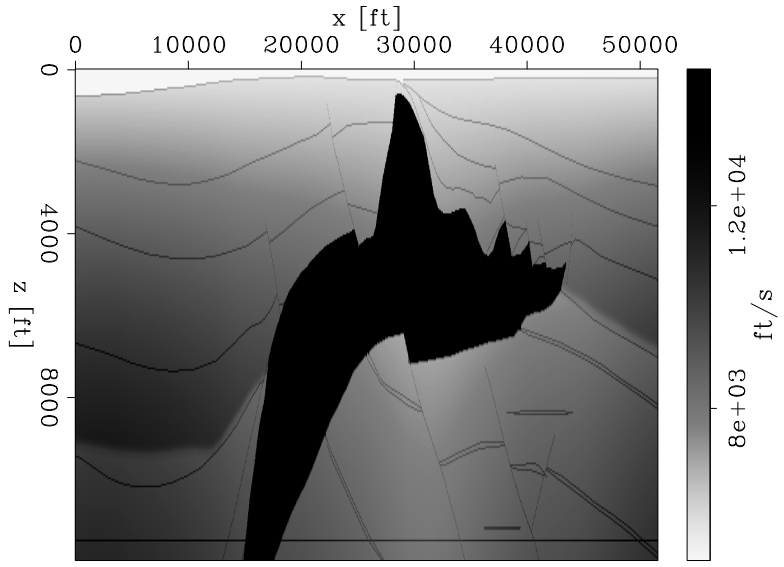

Figure 1: The 2D SEG/EAGE velocity model for the salt-dome example. huazhong1-salt_model [ER]

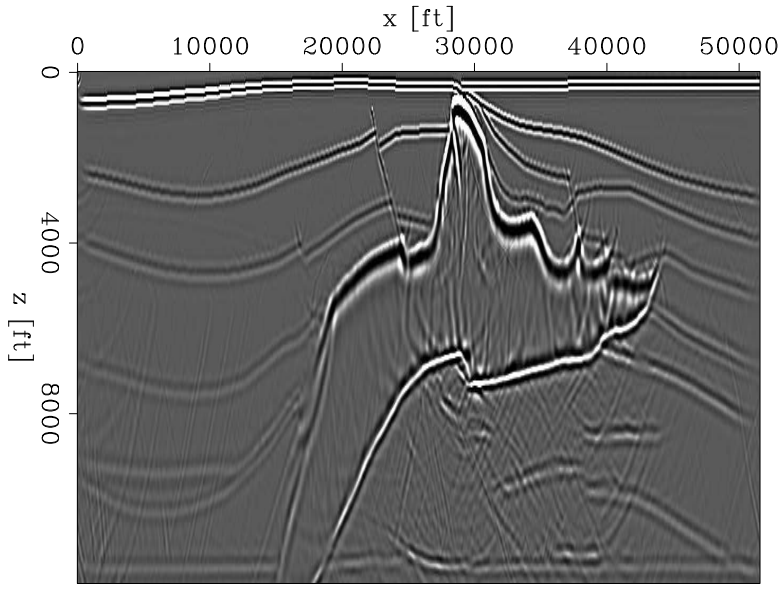

Figure 2: The imaging result of 2D poststack depth migration with one reference velocity during an extrapolation step. huazhong1-single_ref_v [ER]

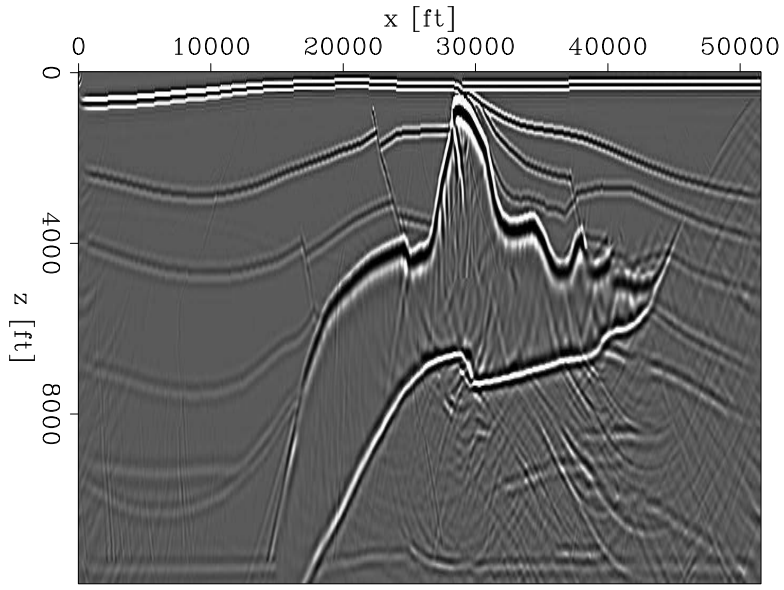

Figure 3: The imaging result of 2D poststack migration with a set of reference velocities during an extrapolation step with a threshold of 1.5. huazhong1-multiple_ref_v1.5 [ER]

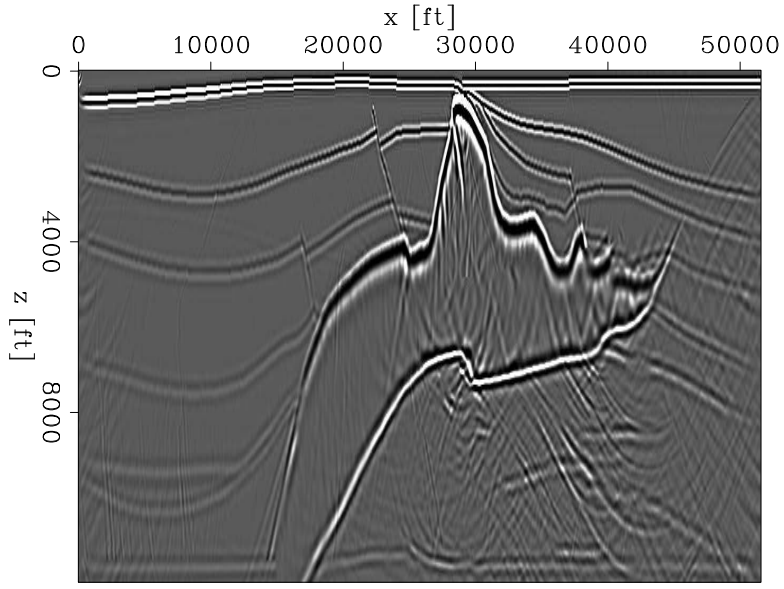

Figure 4: The imaging result of 2D poststack migration with a set of reference velocities during an extrapolation step with a threshold of 1.3. huazhong1-multiple_ref_v1.3 [ER]

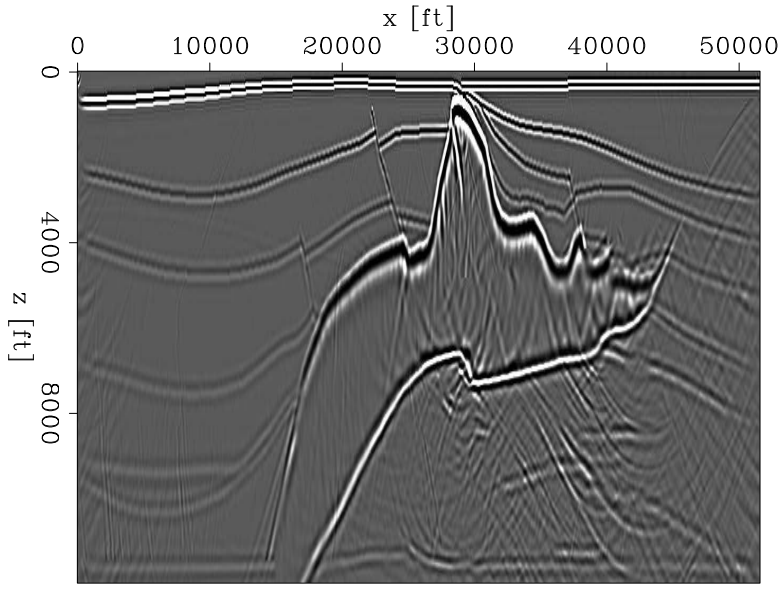

Figure 5: The imaging result of 2D poststack migration with a set of reference velocities during an extrapolation step with a threshold of 1.1. huazhong1-multiple_ref_v1.1 [ER]

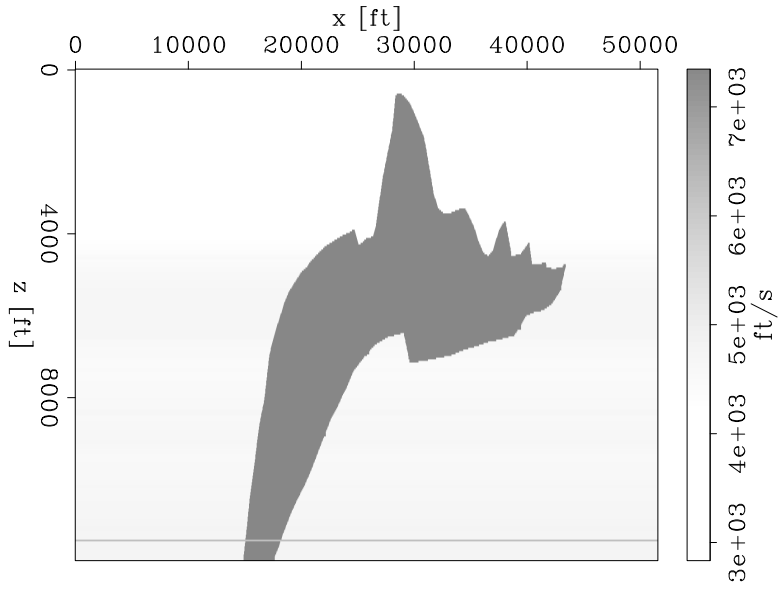

Figure 6: The chosen reference velocity field with a threshold of 1.5 which satisfactorily characterizes the background variation of the true 2D SEG/EAGE salt-dome velocity model. huazhong1-reference_v1.5 [ER]

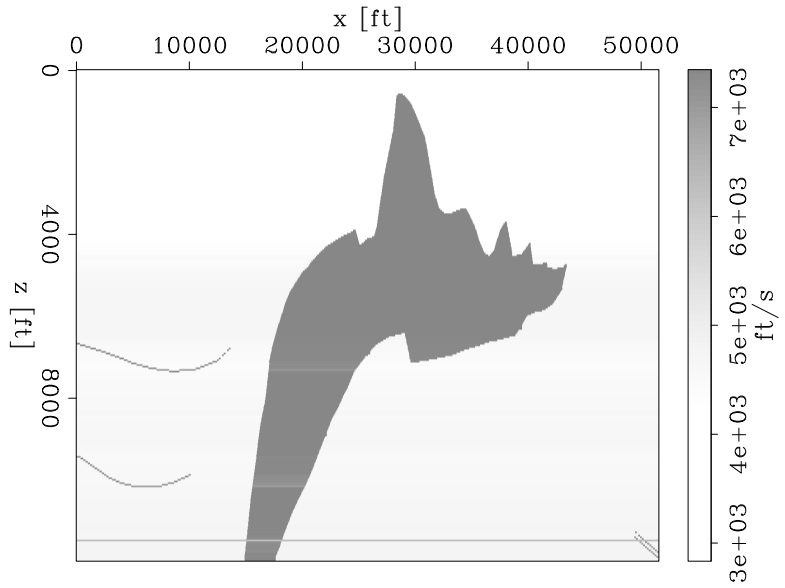

Figure 7: The chosen reference velocity field with a threshold of 1.3 which satisfactorily characterizes the background variation of the true 2D SEG/EAGE salt-dome velocity model. huazhong1-reference_v1.3 [ER]

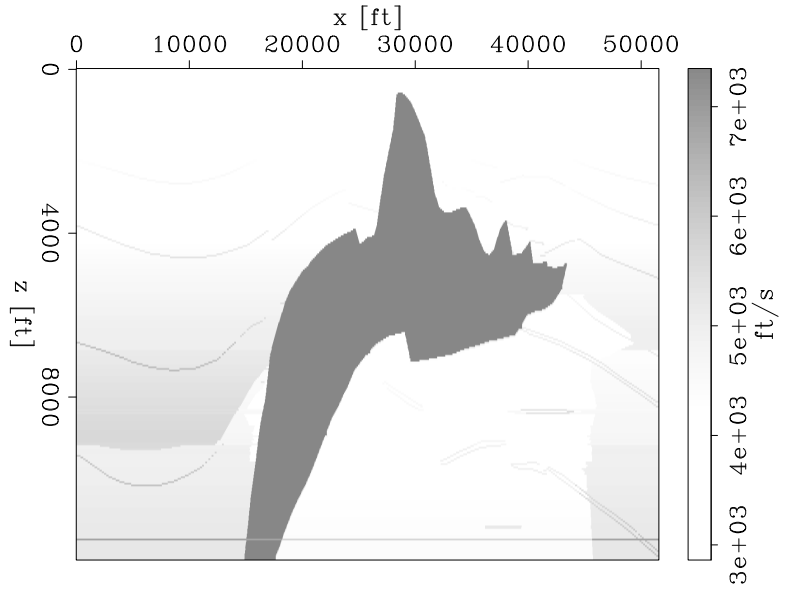

Figure 8: The chosen reference velocity field with a threshold of 1.1 which satisfactorily characterizes the background variation of the true 2D SEG/EAGE salt-dome velocity model. huazhong1-reference_v1.1 [ER]

ACKNOWLEDGEMENT

The first author thanks the SEP Group at Stanford University for providing an opportunity for him to serve as a visiting scholar.

REFERENCES

Biondi, B., 2002, Stable wide-angle Fourier finite-difference downward extrapolation of 3-D wavefields: Geophysics, **67**, 872–882.

Claerbout, J., 1985, Imaging the earth's interior Blackwell Scientific Publications, Oxford., 159–160.

Clapp, R. G., 2004, Reference velocity selection by a generalized lloyd method: 74th Ann. Internat. Mtg., Soc. Expl. Geophys., Expanded abstracts, 981–984.

Gazdag, J., and Sguazzero, P., 1984, Migration of seismic data by phase-shift plus interpolation: Geophysics, **49**, 124–131.

Huang, L. Y., Fehler, M. C., and Wu, R. S., 1999, Extended local Born Fourier migration method: Geophysics, **64**, 1524–1534.

Kessinger, W., 1992, Extended split-step Fourier migration *in* 62nd Ann. Internat. Mtg. Soc. of Expl. Geophys., 917–920.

Ristow, D., and Ruhl, T., 1994, Fourier finite-difference migration: Geophysics, **59**, 1882–1893.

Rousseau, J. H. L., and de Hoop, M. V., 2001, Modeling and imaging with the scalar generalized-screen algorithms in isotropic media: Geophysics, **66**, 1551–1568.

Stoffa, P. L., Fokkema, J. T., de Luna Freire, R. M., and Kessinger, W. P., 1990, Split-step Fourier migration: Geophysics, **55**, 410–421.